Investigations of microwave stimulation of a turbulent low-swirl flame

Ehn, A.; Petersson, P.; Zhu, J. J.; Li, Z. S.; Aldén, M.; Nilsson, E. J K; Larfeldt, J.; Larsson, A.; Hurtig, T.; Zettervall, N.; Fureby, C.

Published in:
Proceedings of the Combustion Institute

DOI:
10.1016/j.proci.2016.06.164

2017

Document Version:
Peer reviewed version (aka post-print)

This is the peer reviewed version of the following article: [1], which has been published in final form at https://doi.org/10.1016/j.proci.2016.06.164

[1] A. Ehn, P. Peterson, J. J. Zhu, Z. S. Li, M. Aldén, E. J. K. Nilsson, J. Larfeldt, A. Larsson, T. Hurtig, N. Zettervall, C. Fureby, "Investigations of Microwave Stimulation of a Turbulent Low-Swirl Flame", Volume 36, Issue 3, Pages 4121-4128 (2017)

Title page

Investigations of Microwave Stimulation of a Turbulent Low-Swirl Flame

A. Ehn[¶*], P. Petersson[¶], J.J. Zhu[¶], Z.S. Li[¶], M. Aldén[¶], E.J.K. Nilsson[¶], J. Larfeldt[‡], A. Larsson[†], T. Hurtig[†], N. Zettervall[†] & C. Fureby[†]

[¶]Division of Combustion Physics, Lund University,
PO Box 118, SE-221 00 Lund, Sweden

[‡]Siemens Industrial Turbomachinery AB.,
SE-612 83 Finspång, Sweden

[†]Defence Security Systems Technology, The Swedish Defence Research Agency – FOI,
SE 147 25 Tumba, Stockholm, Sweden

* Corresponding author: Andreas Ehn
Division of Combustion Physics, Lund University, Sweden
Box 118, S-221 00, Lund, Sweden
Fax: + 46 46 222 45 42
Phone: + 46 46 222 39 28
Email: andreas.ehn@forbrf.lth.se

Abstract

Irradiating a flame by microwave radiation is one of several Plasma-Assisted Combustion (PAC) technologies that can be used to modify the combustion chemical kinetics in order to improve flame-stability and to delay lean blow-out. One practical implication is that engines may be able to operate with leaner fuel mixtures and have an improved fuel flexibility capability including biofuels. In addition, this technology may assist in reducing thermoacoustic instabilities that may severely damage the engine and increase emission production. To examine microwave-assisted combustion a combined experimental and computational study of microwave-assisted combustion is performed for a lean, turbulent, swirl-stabilized, stratified flame at atmospheric conditions. The objectives are to demonstrate that the technology increases both the laminar and turbulent flame speeds, and modifies the chemical kinetics, enhancing the flame-stability at lean mixtures. The study combines experimental investigations using hydroxyl (OH) and formaldehyde (CH_2O) Planar Laser-Induced Fluorescence (PLIF) and numerical simulations using finite rate chemistry Large Eddy Simulations (LES). The reaction mechanism is based on a methane (CH_4)-air skeletal mechanism expanded with sub-mechanisms for ozone, singlet oxygen, chemi-onization, electron impact dissociation, ionization and attachment. The experimental and computational results show similar trends, and are used to demonstrate and explain some significant aspects of microwave-enhanced combustion. Both simulation and experimental studies are performed close to lean blow off conditions. In the simulations, the flame is gradually subjected to increasing reduced electric field strengths, resulting in a wider flame that stabilizes nearer to the burner nozzle. Experiments are performed at two equivalence ratios, where the leaner case absorbs up to more than 5% of the total flame power. Data from experiments reveal trends similar to simulated results with increased microwave absorption.

Keywords: Plasma-Assisted Combustion; Large Eddy Simulations; Laser-Induced Fluorescence; Turbulent Combustion.

1. Introduction and Background

Plasma-Assisted Combustion (PAC) has potential for combustion control and for reducing emissions to meet the globally growing demands on flexible power generation, [1]. Plasma, the fourth state-of-matter, can be used for fuel-reforming and flue-gas treatment, [2-3], but the focus of the present work is on applying the electric energy directly to the flame. PAC offers a method to modify the thermal and kinetic properties of the reactants, intermediates, radicals and products, [4]. Due to fast electron impact excitation and dissociation of molecules at low temperatures, plasma introduces new reaction pathways, modified chemical time-scales, and may significantly change the combustion process, [4-5]. Employing PAC improves flame stability and delays lean blow-out, allowing stable combustion with leaner, low-emission fuel-mixtures. PAC may extend the fuel compatibility to open up for using e.g. bio-fuels with minimal hardware modification.

Different technologies may be used to supply electrical energy to the flame including Dielectric Barrier Discharges (DBD), [6], Gliding Arc Discharges (GAD), [7], Microwave Discharges (MD), [8], and Radio-Frequency Discharge (RFD), [9], as described in [4-5]. Adding electric energy through microwave radiation is advantageous for direct stimulation of a flame since there is no need for electrodes (surviving in the harsh environment in a flame). In addition, microwave irradiation will be most efficiently absorbed in the flame-front, where both the electron density and the reduced electric field, E/N, are high. Creating a microwave-plasma is energy-costly, and here we instead endeavor to use microwave irradiation to generate a plasma-like state below dielectric breakdown. This allows us to influence the flame chemistry mainly by increasing the energy of the electrons already produced by chemiionization, a technology previously explored by Ward, [10]. Several experimental and computational investigations have been performed for microwave-stimulated laminar flames below dielectric breakdown, [11-13], but no previous experimental or computational studies of microwave-stimulation on turbulent swirl-stabilized flames in industrially relevant burners have been found by the authors.

This investigation concerns microwave-stimulated combustion in a lean swirling stratified

turbulent flame at atmospheric conditions. The objectives are to demonstrate that the technology increases both the laminar and turbulent flame speeds and modifies the chemical kinetics so as to enhance flame stability at lean mixtures. A skeletal reaction mechanism for methane (CH_4)-air combustion, expanded with sub-mechanisms for singlet oxygen, ozone, chemionization, electron impact dissociation, ionization and attachment is developed and as a first step applied to laminar flame simulations. The low-swirl flame is studied in an experimental investigations using hydroxyl (OH) and formaldehyde (CH_2O) Planar Laser-Induced Fluorescence (PLIF) and numerical simulations using finite rate chemistry Large Eddy Simulations (LES), [14]. Common trends in experiments and simulations results are used to demonstrate and explain some aspects of microwave-stimulated combustion.

2. Experimental Set-Up and Measuring Technique

This investigation of microwave assisted turbulent combustion is performed for flames stabilized by a low-swirl burner, [15], offering a good compromise between simplicity and flow complexity. The low-swirl flow is created by an outer annular swirler, with eight swirl-vanes, in combination with an inner perforated plate, Fig. 1a. With this design the swirl and the highest velocities are found in the outer part of the flow discharging from the nozzle, [16]. The diverging turbulent flow creates an inner low-velocity region in which the flame is stabilized. The study is performed with the low-swirl burner discharging into a purposely-designed microwave cavity, Fig. 1b, enclosing an air-co-flow of 0.4 m/s. The setup is similar to that used by Ehn *et al*., [17-18], and includes calibrated mass-flow controllers for CH_4 and air (Bronckhorst Hi-Tec, EL-Flow) and a flow-meter for the co-flow (Fox, Thermal Instruments). Equivalence ratios of ϕ=0.58 and 0.62, with theoretical powers of ~24 and ~27 kW, respectively, were studied.

The microwave system includes a magnetron (National Electronics GA15MP) operating at a frequency of 2.45 GHz, a circulator and a load, sensors for incident and reflected power and a three-stub tuner. The flame is kept in a (D=300 mm) metallic cavity to achieve the mode-pattern

that balances the position of the flame, and to obtain proper microwave coupling, Fig. 1c. Microwave coupling to the flame is achieved by tuning the location of the upper metallic grid at the upper end of the cavity, Fig. 1b. The lower metallic grid, positioned between the burner nozzle and the flame, is required to close the microwave cavity but also affects the flow by reducing the swirling motion, resulting in flame stabilization further downstream than reported, [15]. The microwave cavity is purposely designed for OH and CH_2O PLIF measurements with a slit for laser-beams, a built-in beam-dump and a viewport for 90°-angle imaging.

The experimental system is summarized in Fig. 1d: A frequency tripled Brilliant B laser (Quantel), providing 355 nm laser pulses with a pulse duration and pulse energy of approximately 5 ns and 110 mJ, respectively, was employed to probe CH_2O. The Q1(8) transition in the $A^2\Sigma^+ \leftarrow X^2\Pi$ system of OH was probed using a wavelength of ~283 nm with a pulse energy of around 10 mJ and a pulse duration of around 5 ns. The lasers and imaging systems were overlapped using dichroic mirrors. Laser sheets of 5 cm height were focused in the center of the low-swirl burner flame using a combination of cylindrical lenses (fused silica) with focal lengths of 1000 mm and -40 mm, respectively. The CH_2O signal was detected using an ICCD camera (Andor Technologies Istar 334T) equipped with a 50 mm f/1.2 Nikon lens in combination with double (1 mm thick) GG400 Schott filters for laser-light discrimination. The OH signal was spectrally isolated by an UG 11 filter, mounted on a 100 mm fused silica lens (Carl Zeiss F/4.0). The OH signal was captured by a CCD camera (Hamamatsu) operating together with an intensifier (Hamamatsu) optimized for UV. A high-speed video camera (Fastcam SA-Z, Photron) was used to capture high-speed video images of the flame. The optical arrangement is described in more detail by Ehn *et al.* in [17-18].

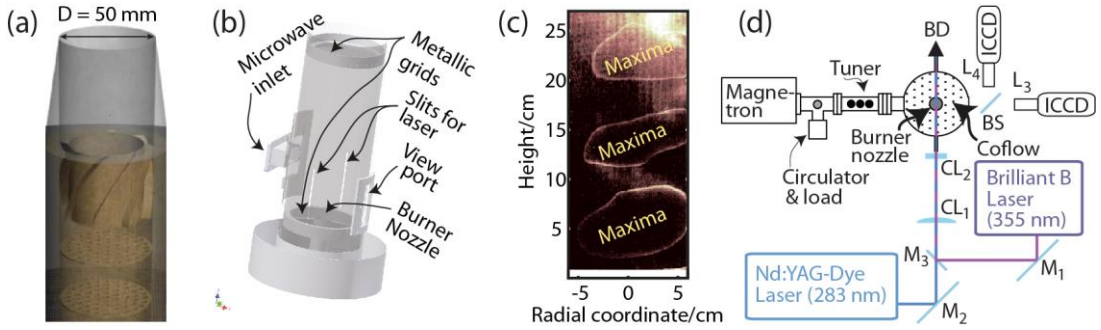

Figure 1. (a) Semitransparent sketch of the low-swirl burner. (b) Cavity housing for the microwaves. (c) Microwave mode pattern inside the cavity around the centerline of the burner. (d) Experimental setup overview including optical arrangements and the microwave system (BD = beam dump, BS, beam splitter, M_1 and M_2 are mirrors and M_3 is a dichroic mirror and L_i are lenses).

3. Large Eddy Simulation Models, Kinetics and Numerical Methods

The simulation model is based on finite-rate chemistry LES, [14], using the Partially Stirred Reactor (PaSR) combustion model, [19], which is extensively validated, e.g. [20], and frequently utilized in applied studies, e.g. [21]. The LES model is implemented in OpenFOAM, [22], and the LES transport equations are solved by using high-order monotonicity-preserving convective and diffusive flux-reconstruction schemes and Crank-Nicholson time-integration, [23]. The combustion chemistry is separately integrated using a Strang-type operator-splitting scheme, [24]. A fully compressible Pressure-based Implicit Splitting of Operators (PISO), [25], algorithm is utilized for the pressure-velocity-density coupling. Stability is enforced by using compact stencils and by enforcing conservation of kinetic energy with a Courant number<0.5.

The microwave-assisted CH_4-air combustion chemistry is modeled using a dedicated skeletal mechanism, Z80, comprising 80 irreversible reactions, consisting of a 42-step CH_4-air mechanism, Z42, combined with reaction sub-sets for ozone, singlet oxygen, chemionisation, electron-impact, and electron attachment and dissociation according to Table S1. The combustion chemistry is sufficiently detailed to describe important flame properties, but small enough for finite-rate chemistry LES. The mechanism development was performed using the laminar flame speed (s_u), flame temperature (T_{flame}) and species concentration profiles of major and other

key species, as targets. Ignition delay times (τ_{ign}) and extinction strain rates (σ_{ext}) were evaluated to characterize the effects of microwave irradiation at different equivalence ratios.

The Z42 CH_4-air mechanism, R1-R35, was adopted from [26], with the addition of CH and CH_2 reactions, R36-R42, from [27], with small modifications to some of the pre-exponential factors. Z42 show excellent agreement with the GRI 3.0 reaction mechanism, [28].

Microwave-stimulated combustion involves reactions of ozone (O_3) and excited oxygen in the singlet state (O_2^*), both known to increase the reactivity of CH_4-air mixtures, [29-30]. The O_3 subset, R43-R55, was selected from Wang *et al.*, [29], as previously used by Ehn *et al.*, [31]. The O_2^* subset, consisting of R56 and R57-R64 from [30], is a dominant source of radicals (H, OH, HO_2 and O) and therefore largely determines the reactivity of the system.

Chemionization provides the background electron concentration, existing also without microwaves, and is here represented by reactions R65-R68, with $CH+O \rightarrow HCO^+ + e$ usually considered as the main chemionization source in flames, e.g. [32].

Electron impact dissociation and ionization reactions, R69-R76, provide radicals by collisions with free electrons, e, and have a highly non-linear dependence on E/N. The ionization reactions contribute significantly to the increasing electron concentration at higher E/N, resulting in increased O_2^* concentration and increased reactivity of the system. All E/N dependent reaction rates, R56 and R69-R76, were determined using BOLSIG+, [33], with cross-sections from Morgan, [34], and Phelps, [35]. Relevant rates for reactions involving electrons require that species with high concentration or large cross-section for low energy electron interactions are taken into account, including inert N_2. These reaction rates were calculated for compositions representative of where CH has the highest concentration. The reaction rate of R56, $O_2+e \rightarrow O_2^*+e$, implemented in the mechanism is decreased compared to the value determined by BOLSIG+. In a more extensive mechanism, collisional quenching would disable some O_2^*, whereas in this simplified mechanism, tuning of O_2^* production is necessary. Sensitivity analysis, reveals that among the E/N dependent reactions the primary flame enhancing reactions are R56 and R74, emphasizing

the significance of the oxygen chemistry in discharge plasma under prevailing conditions. It is, however, interesting to notice that for lean conditions at E/N=80 Td, the E/N dependent reactions are of comparably low importance, and that R57, R61 and R63 from the O_2^* subset have more significant sensitivity.

The electron attachment and dissociation reactions, R77-R80, [36], result in a reduced radical pool since they remove the positive ions created by ionization.

Laminar microwave-assisted flames, at 1 atm and 300 K, were computed, using Chemkin, [37], and the Z80 mechanism at E/N=0, 60, 70 and 80 Td, Fig. 2a. An ideal microwave mode-shape is assumed. Previous results indicate that the increase in s_u, at E/N<125 Td, can be expected to be in the range from 19% to 68%, represented by the shaded area in Fig. 2a. The present modeling suggests that s_u show the smallest relative increase at ϕ=1.0. For reduced electric fields E/N=60 Td, significant enhancement is observed at lean conditions, ϕ<0.8, with more than 50% at ϕ=0.5, reducing to 25% at ϕ=0.6. For E/N=70 Td, the enhancement in s_u at ϕ=0.6 is 120%, decreasing to about 25% at ϕ=1.0. Stronger enhancement, but similar trends, are noted for E/N=80 Td. This is in agreement with Ju *et al.*, [13], in that the flame enhancement is most noticeable at lean conditions. Sensitivity analysis show that the reactions dominating the flame chemistry is strongly dependent on equivalence ratio; for E/N=60 Td the CH_4-air reactions of the Z42 baseline mechanism dominate the chemistry at ϕ=1.0, whereas at lean conditions, reactions of O_2^*, primarily with e, are significantly more important.

Extinction strain-rate computations, Fig. 2b, show a relatively stronger augmentation at lean conditions. Ignition delay times are identical with and without microwaves at temperatures above about 1500 K, while at lower temperatures the ignition occurs considerably faster as the microwave field is applied. This is a result of a strongly increased reactivity at low temperatures where the CH_4-air gas mixture is relatively unreactive otherwise.

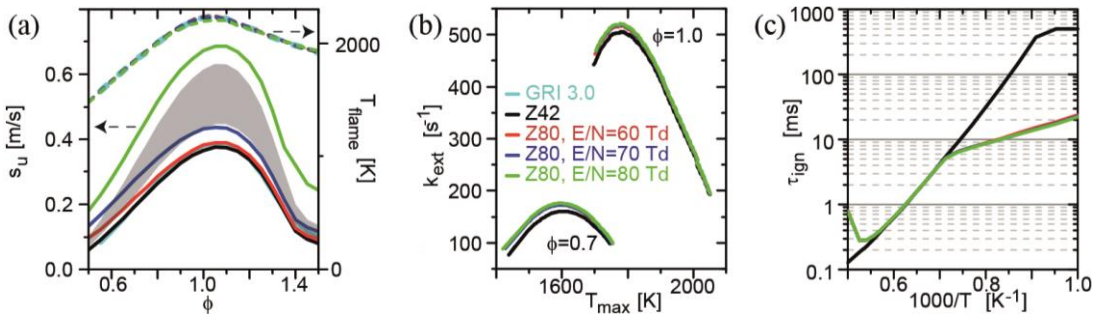

Figure 2. Comparison of (a) adiabatic flame temperatures, T_{ad}, and laminar flame speeds, s_u (b) extinction strain rate, σ_{ext}, and (c) ignition delay times, τ_{ign}, for E/N=0, 60, 70 and 80 Td.

4. Results and Discussion

The design of the burner swirler arrangement, [15], causes an enclosed low-velocity zone to develop within the funnel-shaped swirling CH_4-air flow that rotates in a plane normal to the axial flow. The rotation causes the outer diameter of the funnel-shaped swirling flow to grow with concomitant decrease in axial velocity. The flame is established where the local CH_4-air mixture velocity equals the turbulent flame speed, s_t. The resulting swirling flow exiting the nozzle gives rise to distinctive outer- and inner shear-layers that gradually expands and strengthens the downstream mixing. Consequently, the flame is comprised of a turbulent premixed undulating flame-cup followed by a progressively stratified plume interacting largely with the inner shear-layer. Based on assessments of the Damköhler and Karlowitz numbers, the flame unveils many flame front topologies including (i) wrinkled flamelets at the flame-cup, (ii) corrugated flamlets at the lower part of the flame, and (iii) thin reaction-zones at the upper part of the flame due to the gradual stratification and intermittent interactions with the shear-layers.

Microwave stimulation does not change the overall behavior of the flame, but modifies its position, width and intensity, particularly in the flame-cup and lower part of the flame, as demonstrated experimentally in Fig. 3a-3b, and computationally in Fig. 3c-3f. Figures 3a and 3b show high-speed images with and without microwave stimulation, respectively. This is line-of-sight data and is thus the integrated signal of flame chemiluminescence. In addition to an obvious increase in flame chemiluminescence with microwave stimulation the flame becomes wider

and moves somewhat closer to the burner nozzle. This effect on the flame is seen in the snapshot images in Fig. 3a and 3b, which is further seen in the averaged optical measurement data. Moreover, exhaust temperature monitoring using a thermocouple, 11 D above the burner, reveal up to 10% increase in gas temperature when ~2 kW electric energy is absorbed by the flame at ϕ=0.58.

Volumetric renderings from LES at E/N=0, 60, 70 and 80 Td are presented in Fig. 3c, 3d, 3e and 3f, respectively. The volumetric renderings are composed of the temperature, T, CH_4, CH and O_2^*. The microwave-simulated flames indicate similar behavior compared to the experimental visualizations in Fig. 3a and 3b, in that the flame stabilize closer to the burner nozzle, and also that the flame volume and area increase with increased E/N. In all cases, CH is found in a thin wrinkled layer in the flame front, whereas gradually increasing levels of O_2^* with increasing E/N are found in the whole flame for the microwave-stimulated cases. Moreover, the average temperature in the post flame region (about 10D above the burner nozzle) shown an increase by ~10% for E/N=60 to 70 Td, and about 20% for E/N=80 Td.

From the laminar flame speed results in Fig. 2a it is apparent that microwave stimulation causes the laminar flame speed, s_u, to increase non-linearly in the E/N range of interest, whereas the flame temperature, T_{flame}, remains virtually unaffected by microwave irradiation. In the LES the flame-cup moves closer to the burner nozzle with increasing E/N, in a similar non-linear way as the increase in s_u in the laminar flame. All in all, this suggests that the microwave irradiation primarily interacts with the chemical kinetics. The increase in s_u and s_t widens the lower parts of the flame, which then interacts more strongly with the annular shear layer discharging from the burner. Such interactions increase the flame wrinkling and flame area, which together with the anisotropy of the flow discharging from the burner results in that the lateral turbulent flame speed increases faster than the vertical turbulent flame speed.

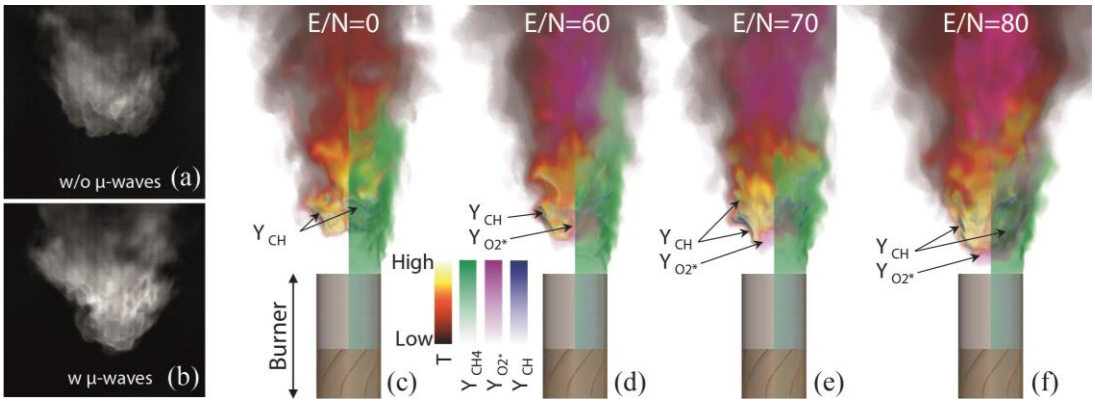

Figure 3. Typical experimental images without (a) and with (b) microwave-stimulation. Volumetric renderings of T, CH_4, CH and O_2^* from LES at ϕ=0.6 and E/N=0, 60, 70 and 80 Td are presented in panels (c) to (f).

Time-averages and rms-fluctuations of the axial velocity, v_x, and T are shown in Fig. 4a and 4b, respectively, athwart the flame at different heights above the burner. Here, experimental data, [15-16, 38], are compared with LES predictions, without microwave irradiation at ϕ=0.62. Acceptable agreement between experimental data and LES predictions in terms of temperature and axial velocity fields are noticeable, making the low-swirl flame a suitable case for this combined experimental and computational investigation of microwave assisted combustion. Regarding the time-averaged axial velocity, $\langle v_x \rangle$, only minor differences between the LES and experimental profiles may be observed. The experimental data presents a somewhat more narrow v_x funnel at 0.20<x/D<0.50, and a somewhat weaker recirculation region at 0.60<x/D<1.20, where also the time-averaged temperature. $\langle T \rangle$, differ due to a slight difference (<5%) in flame lift-off height. In addition, there are discrepancies concerning the axial rms-velocity fluctuations, v_x^{rms}, but still remaining within the experimental uncertainty, and focused around the region of flame anchoring, around x/D=0.60, signifying that they are related to the small offset in lift-off height, which is also clear from the temperature rms fluctuations, T^{rms}, in this region. LES predictions for the ϕ=0.6 case with E/N=0, 60, 70 and 80 Td are presented to investigate the effects of microwaves. This flame condition is very close to lean-blow off and is thus selected to demonstrate the influence of microwave-stimulation. For E/N=80 Td, the widening of the flame is seen in

both $\langle v_x \rangle$ and $\langle T \rangle$ at 0.80<x/D in the cross-sectional data at ϕ=0.6. The temperature, T, shows that the flame stabilizes closer to the burner nozzle, especially for E/N=80 Td at x/D=0.2 and 0.5.

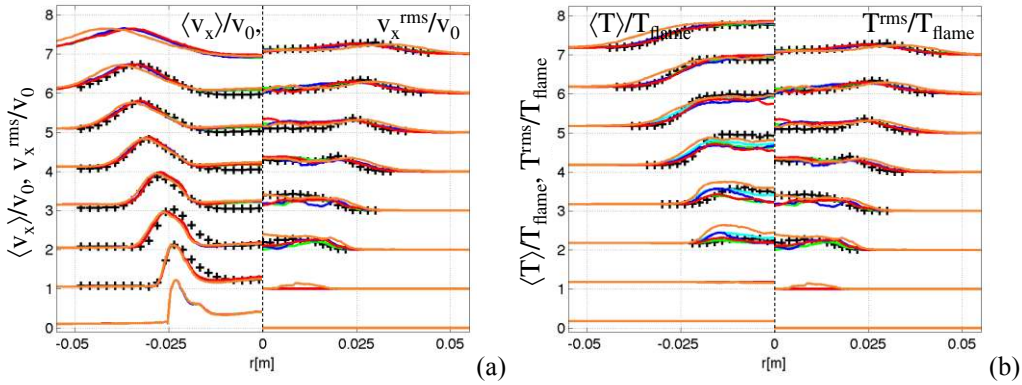

Figure 4. Cross-sectional comparison of (a) time-averaged axial velocity, $\langle v_x \rangle$, and rms-velocity fluctuations, v_x^{rms}, and (b) time-averaged temperature $\langle T \rangle$ and rms-temperature fluctuations, T^{rms}, at h/D=0, 0.2, 0.5, 0.6, 0.8, 1.0, 1.2 and 1.6. Legend: (+) experimental data (from [15-16, 38]) for ϕ=0.62 and E/N=0 Td, (—) LES predictions at ϕ=0.62 and E/N=0 Td. LES predictions at ϕ=0.60 and: (—) E/N=0 Td, (—) E/N=60 Td, (—) E/N=70 Td and (—) E/N=80 Td.

Time-averaged number densities from LES results and PLIF signals of CH_2O and OH data are shown in Fig. 5b and 5c, at ϕ=0.6 and E/N=0, 60, 70 and 80 Td, respectively. It is important to note that the LES are based on a model in which the flame is exposed to a spatially limited constant reduced electric field that can be altered, while the electric field mode-pattern in the current experimental set-up is affected by the turbulent flame and is thus varying. The temperature of the flame results in a non-uniform reduced electric field. Hence, quantitative comparison between experiments and simulations should be carried out with care. Instead, however, results from the two approaches are compared in terms of trends in the flame behavior.

Experimentally, flames at ϕ=0.58 and 0.62 were studied with the leaner flame being very close to the lean blow-off limit. The intensity of the cross-sectional data should not be compared between the two experimental datasets. The windows used for comparison are emphasized by the box in Fig. 5a, and the corresponding PLIF and LES images, in Fig. 5b and 5c are mirrored at the centerline. Figure 5a shows volumetric renderings of T, CH_2O and OH, O and O_2^*, whereas

Fig. 5d shows a reaction path diagram for Z80. Singlet oxygen (O_2^*) exist in the whole flame for E/N>0, whereas CH only exist in the flame front. Formaldehyde (CH_2O) mainly exists in the pre-heat layer and in the post-flame zone, and for E/N>70 Td broadening of the CH_2O layer is observed following the strengthened flame shear-layer interactions. OH and O exist concurrently and increase with higher E/N, whilst partly concealing the CH_2O distribution due to their wider and intertwined distributions around the flame-cup. In addition, the high T flame zone is growing with increasing E/N.

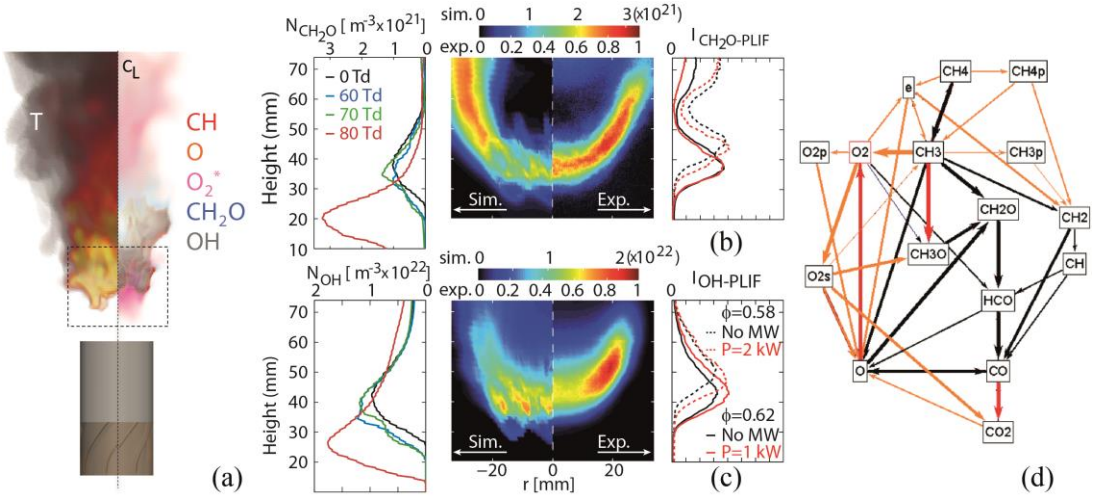

Figure 5. (a) Volumetric renderings of T, (left) and an overlay of CH_2O, OH, CH, O and O_2^* (right) at E/N=70 Td. The dashed box designates the image area where LES results and PLIF data are shown in (b) and (c). Time-averaged LES and PLIF images of OH and CH_2O are shown in (b) and (c), respectively, together with radially averaged profiles. (d) Reaction path diagram for Z80 in Table S1.

Time-averaged LES number densities at E/N=70 Td agree with the mean PLIF CH_2O and OH distributions with 1 kW absorption, according to Fig. 5b and 5c. Still, the positions of the mean OH and CH_2O signals, seen by comparing the cross-sectional data, is somewhat higher for the experimental data due to the metallic grid that is position just above the burner nozzle. The LES profiles are clearly shifted, in particular for CH_2O, when E/N is increased from 70 Td to 80 Td. Reduced field strengths of 60 Td and 70 Td also brings the flame closer to the burner nozzle that is also seen in the experimental cross-sectional profiles for ϕ=0.58. However, this is not observed for the ϕ=0.62 case, which is a combination of decreased microwave coupling to the

flame, and that the flame is less stable at leaner conditions. Experimental data reveal a modest increase in CH_2O signal for ϕ=0.58, and virtually no effect at ϕ=0.62, whereas a clear increase is seen for the OH signal in both data sets. Such behavior is also observed in the LES profiles with E/N=60 and 70 Td where the increase in CH_2O data is less pronounced than for OH.

The microwaves stimulate the formation of electrons by means of electron impact dissociation and ionization, provided a background of electrons. The electrons are first created at the microwave maxima and multiplied by electron impact ionization. O_2^* is formed through collisions between e and O_2. In this premixed case, where O_2 is abundant, O_2^* will have largest production rates where the electrons are accelerated by the reduced electric field. The reaction path diagram in Fig. 5d reveals the most important connection between the species, where the reaction paths in the CH_4-air subset (Z42) is represented by black and red arrows, and the orange arrows belong to reaction paths activated by microwaves. Red arrows indicate important reaction paths in CH_4-air combustion enhanced by microwaves. The importance of CH_3O is increased as a result of microwaves. Production of CH_2O via CH_3O becomes dominating by O_2^* reacting with CH_3, meaning that O_2^* indirectly contributes to enhanced reactivity. O_2^* contribute to CH_2O production via CH_3O and is also important for O production that eventually lead to CH_2O. This implies that microwave-assisted combustion provide new routes to CH_2O formation. On the other hand, HCO is mainly formed directly from CH_2O, just like for normal CH_4-air combustion. Production of OH is connected to the increased reactivity of the system, which is mainly enhanced by O_2^*, being the key species for microwave enhanced CH_4-air combustion.

5. Concluding Remarks

Microwave stimulation of a swirl stabilized flame has been experimentally and computationally examined with PLIF and combustion LES. Similar trends are seen from simulations and experiments for cases close to the lean blow-off limit. Microwave stimulation increased flame-area, flame-volume and exhaust gas temperature as well as making the flame stabilize closer to the burner nozzle. These trends indicate an increase in turbulent flame speed, which is in line with

the fact that microwave stimulation increases the laminar flame speed. In addition, the microwaves clearly increase the concentration of OH in the post-flame region. Laminar flame simulations identify the production of singlet oxygen (O_2^*) to be the most dominant species in the flame speed enhancement. The production of O_2^* in the turbulent flame is highly nonlinear in relation to E/N and is much more efficient at higher reduced electric fields. LES predictions indicate that reduced electric field strengths below 70 Td has moderate impact on the flame whereas the nonlinearity in flame speed enhancement is accentuated for reduced electric fields between 70 and 80 Td. However, increasing the microwave power and E/N in a continuous system will result in gas breakdown and excessive heating that in turn will increase NO_x production. This suggests that pulsed microwave stimulation, where high reduced electric fields of several hundred Td and short pulses are generated, would be of interest for plasma-assisting combustion control.

Acknowledgement

This work has been financed by the Swedish Energy Agency and the advanced ERC grant (TU-CLA). Jon Tegnér is acknowledged for assistance with evaluating the reaction mechanisms and Jiajian Zhu would like to thank China Scholarship Council for financial support.

References

[1] S. Chu & A. Majumdar, Nature, **488** (2012) 294-303.

[2] Y. Kim, S. Abbate, H. Ziock, G.K. Anderson & L.A. Rosocha, IEEE Transactions on Plasma Science (2007) **35**, 1677-1681.

[3] H. Lin, Z. Huang, W. Shuangguan & X. Peng, Proc. Comb. Inst. (2007) 31, p 3335-3342.

[4] A. Starikovskiy A. & N. Aleksandrov, Prog. Energy Comb. (2013) 39, p 61-110.

[5] Y. Ju, W. Sun, Prog. Energy Comb. Sci. (2015) 48, 21-83.

[6] A. Vincent-Radonnier, S. Larigaldie, P. Magre & V. Sebelnikov, Plasma Sources Sci. Tech. (2007) 16, 149-160.

[7] I. Matveev, S. Matveeva,A. Gutsol, A. Fridman, Non-Equilibrium Plasma Igniters and Pilots for Aerospace Application, 43rd AIAA aerospace science meeting, Reno, NV, 2005, AIAA-2005-1191.

[8] I. Esakov, L. Grachev, K. Khodataev, D. Van Wie, Experiments on Propane Ignition in High-Speed Airflow using a Deeply Undercritical Microwave Discharge, 42rd AIAA aerospace science meeting, Reno, NV, 2004, AIAA-2004-0840.

[9] A. Mariani, F. Foucher, Appl Energy (2014) 122, 151–161.

[10] M.A.W. Ward, J. Microwave Power (1977) 12, 187-199.

[11] S.H. Zaidi, S.O. Macheret, Y. Ju, R.B. Miles, D.J. Sullivan & P.C. Efthimion, Microwave-Assisted Hydrocarbon Flame Speed Enhancement, 43rd AIAA aerospace science meeting, Reno, NV, 2005, AIAA 2005-0992.

[12] E.S. Stockman, S.H. Zaidi, R.B. Miles, C.D. Carter & M.D. Ryan, Comb. Flame (2009) 156, 1453-1461.

[13] Y. Ju, S.O. Macheret, M.N. Shneider, R.B. Miles & D.J. Sullivan, Numerical Study of the Effect of Microwave Discharge on the Premixed Methane-Air Flame, 40rd AIAA Joint propulsion conference and exhibit, Fort Lauderdale, Florida, 2004, AIAA 2004-3707.

[14] S. Menon & C. Fureby, Computational Combustion, In Encyclopedia of Aerospace Engineering, Eds. R. Blockley & W. Shyy, John Wiley & Sons, 2010.

[15] P. Petersson, J. Olofsson, C. Brackman, H. Seyfried, J. Zetterberg, M. Richter, M. Alden, M.A. Linne, R.K. Cheng, A. Nauert, D. Geyer & A. Dreizler, Applied Optics (2007), 46, 3928-3936.

[16] K.J. Nogenmyr, C. Fureby, X.S. Bai, P. Petersson, R. Collin & M.A. Linne, Comb. Flame (2009), 156, 25-36.

[17] A. Ehn, T. Hurtig, P. Petersson, N. Zettervall, B. Zhou, J. Zhu, Z-S Li, M. Aldén, C. Fureby, A. Larsson & J. Larfeldt, Microwave Stimulated Combustion Investigated by Laser Diagnostics and Chemical Kinetics, 7th European Comb. meeting, Budapest, Hungary,

2015.

[18] A. Ehn, T. Hurtig, P. Petersson, J. Zhu, A. Larsson, C. Fureby, J. Larfeldt, Z-S Li & M. Aldén, 2015, "Setup for Microwave Stimulation of a Turbulent Low-Swirl Flame", submitted to Journal of Physics D: Applied Physics (2015).

[19] V. Sabelnikov & C. Fureby, Comb. Flame, (2013), 160, 83-96.

[20] G. Bulat, E. Fedina, C. Fureby, W. Meier, U. Stopper, Proc. Comb. Inst. 35, (2015), 3175-3183.

[21] N. Zettervall, E. Fedina, K. Nordin-Bates, E.J.K. Nilson & C. Fureby, Combustion LES of a Multi-Burner Annular Aero-engine Combustor using a Skeletal Reaction Mechanism for Jet-A Air Mixtures, 51st AIAA/SAE/ASEE joint propulsion conference, Orlando, FL, 2015, AIAA-2015-4020.

[22] H.G. Weller, G. Tabor, H. Jasak & C. Fureby, Comp. in Physics (1998) 12, 620-631.

[23] D. Drikakis, C. Fureby, F.F. Grinstein & M. Liefendahl, ILES with Limiting Algorithms, In Implicit Large Eddy Simulation: Computing Turbulent Fluid Dynamics, Eds. Grinstein F.F., Margolin L. & Rider B., Cambridge University Press, 2007, p. 94.

[24] E. Hairer & G. Wanner, Solving Ordinary Differential Equations, in II: Stiff and Differential-Algebraic Problems, 2nd Ed., Springer Verlag, 1991.

[25] N.W. Bressloff, Int. J. Num. Methods in Fluids (2001), 36, 497-518.

[26] M.D. Smooke & V. Giovangigli, Formulation of the Premixed and Nonpremixed Test Problems, in Lecture Notes in Physics: Reduced Kinetic Mechanisms and Asymptotic Approximations for Methane-Air Flames, M.D. Smooke (Ed.), 384, Springer-Verlag, New York, 1991, p 1.

[27] I. Glassman, R. A Yetter, "Combustion, Fourth Edition", Elsevier 2010.

[28] F. Frenklach, H. Wang, C.L. Yu, M. Goldenberg, C.T. Bowman, R.K. Hanson, D.F. Davidson, E.J. Chang, G.P. Smith, D.M. Golden, W.C. Gardiner & V. Lissianski, available at http://www.me.berkeley.edu/gri_mech.

[29] Z.H. Wang, L. Yang, B. Li, Z-S Li, Z.W. Sun, M. Aldén, K.F. Cen & A.A. Konnov, Comb. Flame (2012) 159, 120-129.

[30] A.M. Starik, V.E. Kozlov & N.S. Titova, Comb, Flame (2010) 157, 313-327.

[31] A. Ehn, J. Zhu, P. Petersson, Z-S Li, M. Aldén, C. Fureby, T. Hurtig, N. Zettervall, A. Larsson & J. Larfeldt, Proc. Comb. Inst. 35, (2015), 3487-3495.

[32] T. Pedersen, R.C. Brown, Combust. Flame (1993) 94, 433-448.

[33] G.J.M Hagelaar & L.C. Pitchford, Plasma Sources Sci. Techn. (2005) 14, 722-733.

[34] W.L. Morgan, Plasma Chemistry and Plasma Processing (1992) 12, 477-493.

[35] A.V. Phelps (private communication) available at http://jilawww.colorado.edu/~avp/

[36] N.L. Aleksandrova, S.V. Kindyshevaa, E.N. Kukaeva, S.M. Starikovskayab & A.Yu. Starikovskiic, Plasma Physics Reports (2009) 35, 867–882.

[37] CHEMKIN 10112, Reaction Design: San Diego, 2011.

[38] H. Carlsson, E. Nordström, A. Bohlin, P. Petersson, Y. Wu, R. Collin, M. Aldén, P-E Bengtsson,X.-S Bai, Comb. Flame (2014) 161, 2539-2551.

Figure Captions

Figure 1. (a) Semitransparent sketch of the low-swirl burner. (b) Cavity housing for the microwaves. (c) Microwave mode pattern inside the cavity around the centerline of the burner. (d) Experimental setup overview including optical arrangements and the microwave system (BD = beam dump, BS, beam splitter, M_1 and M_2 are mirrors and M_3 is a dichroic mirror and L_i are lenses).

Figure 2. Comparison of (a) adiabatic flame temperatures, T_{ad}, and laminar flame speeds, s_u (b) extinction strain rate, σ_{ext}, and (c) ignition delay times, τ_{ign}, for E/N=0, 60, 70 and 80 Td.

Figure 3. Typical experimental images without (a) and with (b) microwave-stimulation. Volumetric renderings of T, CH_4, CH and O_2^* from LES at ϕ=0.6 and E/N=0, 60, 70 and 80 Td are presented in panels (c) to (f).

Figure 4. Cross-sectional comparison of (a) time-averaged axial velocity, $\langle v_x \rangle$, and rms-velocity fluctuations, v_x^{rms}, and (b) time-averaged temperature $\langle T \rangle$ and rms-temperature fluctuations, T^{rms}, at h/D=0, 0.2, 0.5, 0.6, 0.8, 1.0, 1.2 and 1.6. Legend: (+) experimental data (from [15-16, 38]) for ϕ=0.62 and E/N=0 Td, (—) LES predictions at ϕ=0.62 and E/N=0 Td. LES predictions at ϕ=0.60 and: (—) E/N=0 Td, (—) E/N=60 Td, (—) E/N=70 Td and (—) E/N=80 Td.

Figure 5. (a) Volumetric renderings of T, (left) and an overlay of CH2O, OH, CH, O and O2* (right) at E/N=70 Td. The dashed box designates the image area where LES results and PLIF data are shown in (b) and (c). Time-averaged LES and PLIF images of OH and CH2O are shown in (b) and (c), respectively, together with radially averaged profiles. (d) Reaction path diagram for Z80 in Table S1.

List of Supplementary material

SMM Ehn et al PCI36 2016	A table of reaction parameters for the kinetics mechanism is available as supplementary material (word document).

Table caption in supplementary material

Table S1. Reaction rates for Z80 in the form of Arrhenius expression $k = A \cdot T^n \cdot \exp(-$

E_a/RT) cm^3 mol^{-1} s^{-1}. Units: A – cm^3 mol^{-1} s^{-1}, E_a – cal mol^{-1}, T – K, R = 1.987207 cal K^{-1} mol^{-1}.

Supplementary Material

(Ehn et al. "Investigations of Microwave Stimulation of a Turbulent Low-Swirl Flame", Proc. Combust. Inst. 36, 2016)

Table S1. Reaction rates for Z80 in the form of Arrhenius expression $k = A \cdot T^n \cdot \exp(-E_a/RT)$ $cm^3\ mol^{-1}\ s^{-1}$. Units: A – $cm^3\ mol^{-1}\ s^{-1}$, E_a – cal mol^{-1}, T – K, R = 1.987207 cal $K^{-1}\ mol^{-1}$.

#	*Reaction*	*A*	*n*	E_a
1	CH_4 (+ M) → CH_3 + H (+ M)[a]			
	k_f	6.30E+14	0	104000
	k_{f0}	1.00E+17	0	86000
2	CH_3 + H (+ M) → CH_4 (+ M)[a]			
	k_f	5.20E+12	0	-1310
	k_{f0}	8.25E+14	0	-19310
3	CH_4 + H → CH_3 + H_2	2.20E+04	3	8750
4	CH_3 + H_2 → CH_4 + H	9.57E+02	3	8750
5	CH_4 + OH → CH_3 + H_2O	1.60E+06	2.1	2460
6	CH_3 + H_2O → CH_4 + OH	3.02E+05	2.1	17422
7	CH_3 + O → CH_2O + H	6.80E+13	0	0
8	CH_3 + O_2 → CH_3O + O	5.00E+13	0	25652
9	CH_3 + OH → CH_2 + H_2O	7.60E+06	2	5000
10	CH_3O + H → CH_2O + H_2	2.00E+13	0	0
11	CH_3O + M → CH_2O + H + M	2.40E+13	0	28812
12	CH_2 + O → CO + H_2	3.00E+13	0	0
13	CH_2 + OH → CH + H_2O	1.13E+07	2	3000
14	CH_2O + H → HCO + H_2	9.00E+13	0	3991
15	CH_2O + OH → HCO + H_2O	3.00E+13	0	1195
16	CH + O → CO + H	5.70E+13	0	0
17	CH + OH → HCO + H	3.00E+13	0	0
18	CH + O_2 → HCO + O	3.30E+13	0	0
19	CH + CO_2 → HCO + CO	8.40E+13	0	200
20	HCO + H → CO + H_2	4.00E+13	0	0
21	HCO + M → CO + H + M	1.60E+14	0	14700
22	CO + OH → CO_2 + H	1.51E+07	1.3	-758
23	CO_2 + H → CO + OH	1.57E+09	1.3	21000
24	H + O_2 → OH + O	1.55E+14	0	16800
25	OH + O → H + O_2	1.20E+13	0	690
26	O + H_2 → OH + H	1.80E+10	1	8826
27	OH + H → O + H_2	8.00E+09	1	6760
28	H_2 + OH → H_2O + H	1.17E+09	1.3	3626
29	H_2O + H → H_2 + OH	5.09E+09	1.3	18588
30	OH + OH → O + H_2O	6.00E+08	1.3	0
31	O + H_2O → OH + OH	5.90E+09	1.3	17029
32	H + O_2 + M → HO_2 + M	1.60E+18	-0.8	0
33	H + HO_2 → OH + OH	1.50E+14	0	1004
34	H + HO_2 → H_2 + O_2	2.50E+13	0	700
35	OH + HO_2 → H_2O + O_2	2.00E+13	0	1000
36	HO_2 + HO_2 → H_2O_2 + O_2	8.00E+13	0	0
37	H_2O_2 + M → OH + OH + M	1.30E+17	0	45500
38	OH + OH + M → H_2O_2 + M	9.86E+14	0	-5070
39	H_2O_2 + OH → H_2O + HO_2	1.00E+13	0	1800
40	H_2O + HO_2 → H_2O_2 + OH	2.86E+13	0	32790
41	OH + H + M → H_2O + M	2.20E+22	-2	0

42	$H + H + M \rightarrow H_2 + M$	1.80E+18	-1	0
	Ozone			
43	$O_2 + O + M \rightarrow O_3 + M$	8.60E+13	0	721.3
44	$O_3 + O_2 \rightarrow O_2 + O + O_2$	1.54E+14	0	2.306e+04
45	$O_3 + N_2 \rightarrow O_2 + O + N_2$	4.00E+14	0	2.267e+04
46	$O_3 + O \rightarrow O_2 + O + O$	2.48E+15	0	2.273e+04
47	$O_3 + O_3 \rightarrow O_2 + O + O_3$	4.40E+14	0	2.306e+04
48	$O_2 + O + O_3 \rightarrow O_3 + O_3$	1.67e+15	-0.5	-1391
49	$O_3 + H \rightarrow O_2 + OH$	8.43E+13	0	933.9
50	$O_3 + H \rightarrow O + HO_2$	4.52E+11	0	0
51	$O_3 + OH \rightarrow O_2 + HO_2$	1.85E+11	0	831
52	$O_3 + H_2O \rightarrow O_2 + H_2O_2$	6.62E+01	0	0
53	$O_3 + HO_2 \rightarrow OH + O_2 + O_2$	6.62E+09	0	993.9
54	$O_3 + O \rightarrow O_2 + O_2$	4.82E+12	0	4094
55	$O_3 + CH_3 \rightarrow CH_3O + O_2$	5.83E+10	0	0
	Singlet oxygen			
56	$O_2 + e \rightarrow O_2^* + e$	f(E/N)		
57	$H + O_2^* \rightarrow OH + O$	1.10E+14	0	1.257e+04
58	$OH + O \rightarrow H + O_2^*$	5.80E+12	0	2.454e+04
59	$CH_3 + O_2^* \rightarrow CH_3O + O$	2.11E+13	0	2.852e+04
60	$O_2^* + M \rightarrow O + O + M$	5.82E+21	0	9.539e+04
61	$H_2 + O_2^* \rightarrow H + HO_2$	3.28E+17	0	3.619e+04
62	$OH + O_2^* \rightarrow O + HO_2$	2.39E+16	0	3.396e+04
63	$CO + O_2^* \rightarrow CO_2 + O$	3.14E+12	0	1.447e+04
64	$CH_4 + O_2^* \rightarrow CH_3 + HO_2$	7.59E+12	0	7.2e+04
	Chemiionization			
65	$CH + O \rightarrow HCO^+ + e$	3.00E+11	0	1.5e+04
66	$HCO^+ + H_2O \rightarrow H_3O^+ + CO$	5.00E+15	0	4000
67	$H_3O^+ + e \rightarrow H_2O + H$	2.29E+18	-0.5	2000
68	$H_3O^+ + e \rightarrow H_2 + OH$	1.25E+19	-0.5	4000
	Electron impact dissociation			
69	$O_2 + e \rightarrow O + O + e$	f(E/N)		
70	$H_2O + e \rightarrow H_2 + O + e$	f(E/N)		
71	$CO_2 + e \rightarrow CO + O + e$	f(E/N)		
72	$H_2 + e \rightarrow H + H + e$	f(E/N)		
73	$CH_4 + e \rightarrow CH_3 + H + e$	f(E/N)		
	Electron impact ionization			
74	$O_2 + e \rightarrow O_2^+ + e + e$	f(E/N)		
75	$CH_4 + e \rightarrow CH_4^+ + e + e$	f(E/N)		
76	$CH_3 + e \rightarrow CH_3^+ + e + e$	f(E/N)		
	Electron attachment and dissociation			
77	$O_2^+ + e \rightarrow O + O$	3.6132e+19	-1.0	0
78	$CH_4^+ + e \rightarrow CH_3 + H$	3.0712e+19	-0.5	0
79	$CH_4^+ + e \rightarrow CH_2 + H + H$	3.0712e+19	-0.5	0
80	$CH_3^+ + e \rightarrow CH_2 + H$	6.3231e+19	-0.5	0

[a] Third body efficiencies: CH_4: 6.5, CO:0.75, CO_2:1.5, H_2:1, H_2O:6.5, N_2:0.4, O_2:0.4